Role of curvature elasticity in sectorization and ripple formation during melt crystallization of polymer single crystals

Rujul Mehta,[1] Wirunya Keawwattana,[1] Andrew L. Guenthner,[2] and Thein Kyu[1,*]
[1]*Department of Polymer Engineering, The University of Akron, Akron, Ohio 44325, USA*
[2]*Naval Air Warfare Center, China Lake, California 93555, USA*
(Received 22 July 2003; revised manuscript received 10 November 2003; published 14 June 2004)

The present article focuses on theoretical elucidation of possible effect of mechanical deformation on spatio-temporal emergence of unusual polymer morphology subjected to quiescent isothermal crystallization conditions. The present theory developed is based on a phase field model consisted of non-conserved time dependent Ginzburg-Landau equation having an asymmetric double well potential in the crystal order parameter signifying metastability for crystallization, coupled with the chain tilt angle involving curvature elasticity and strain recovery potentials. Under quiescent crystallization conditions, the curvature elasticity term is needed to discern the emergence of sectorized single crystals. Upon coupling with the strain recovery potential, the numerical calculation captures ripple formation running across the long lamellar growth front, which may be attributed to lamellar buckling caused by the volume shrinkage. Of particular interest is that these simulated topologies of the single crystals are in good accord with the growth character of syndiotactic polypropylene single crystals observed experimentally by us during isothermal crystallization from the melt.

DOI: 10.1103/PhysRevE.69.061802 PACS number(s): 61.41.+e, 81.10.Aj, 87.15.Nn

I. INTRODUCTION

A rich variety of polymer morphology ranging from single crystals to polymer spherulites has been reported over a half century [1–4]. The former has been generally grown from polymer solutions, whereas the latter is commonly produced from the melt by either cooling or thermal quenching below the crystallization temperature. Recently, it has become apparent that some polymer single crystals can be grown from the melt [5] as well. Among them, syndiotactic polypropylene (sPP) shows intriguing single crystal texture with periodic ripples (i.e., corrugated ridges) running across the fastest growing direction of the lamella, i.e., the crystal *b*-axis. A natural question arises as to why the ripples would form in the first place and second why these ridges have to be periodic. The initial explanation was that these periodic ripples might be a consequence of thermal shrinkage of the lamellae during cooling to ambient due to very thin nature of the sPP films [6]. Another conjecture is due to the differential contraction between the lathlike lamellae and the amorphous substrate during anisotropic crystallization [7,8]. Interestingly, the periodic patterns, similar to those of sPP, were observed over 40 years ago in solution-grown truncated single crystals of polyethylene [9], which was attributed to the collapse of the nonplanar pyramid shaped single crystal during solvent evaporation.

There have been numerous theoretical efforts to elucidate polymer crystallization employing diverse approaches. One of the earliest theories for crystallization of low molecular substances from vapor, due to Burton, Cabrera, and Frank [10–12], is called the BCF theory. The BCF theory essentially involves the classical diffusion problem of molecules adsorbed on the crystal surface diffusing towards steps and kinks on the surface. Subsequently, Lauritzen and Hoffman (LH) [13,14] presented a kinetic nucleation theory involving selection of a lamellar thickness that is kinetically most favorable. The LH theory was able to predict the equilibrium lamellar thickness as well as the rate of the crystal growth, especially when the growth rate in all the sectors is uniform. Based on Langevin dynamics, Muthukumar and Welch [15,16] demonstrated that the initial lamellar thickness is controlled by entropic barriers rather than enthalpic factors considered in the LH theory. Moreover, the original LH theory was designed for the prediction of kinetically equilibrated lamellar thickness, and thus it was neither capable of predicting the overall shape of the crystal nor simultaneously predicting the differential growth rates in different sectors of the crystals. As a result, the original LH theory was incapable of describing the emergence of the curved single crystals or anisotropic crystals. Miller and Hoffman [17,18] later modified the LH theory to account for the curved facets in polyethylene single crystals growing through a serrated growth front. Although this modified theory could describe the growth rates of the flat and curved edges of a single crystal, it did not give a full description of the curvature and/or surface textures of the single crystal.

Sadler [19,20] provided a kinetic approach in the context of the surface-roughening concept where new chains deposit on an existing surface in the form of small packets. Whereas any empty site has the same probability to allow deposition of a new packet, probability that desorption will take place at an occupied site depends on the energy of the binding of the packet. An isolated packet will have a high energy of binding, whereas a packet at a kink or a bend has a lower energy. Numerical simulations based on this theory showed appearance of curved growth fronts, but the chief objection to this theory arose from the fact that experiments did not provide any clear evidence to indicate that the crystal surface is rough.

*Corresponding author: tkyu@uakron.edu

Mansfield [21] proposed a dynamic model based on a system of two coupled differential equations based on the Frank's equation [22] to explain the formation of curved single crystals. Point and Villers [23], in order to explain curved crystal growth, provided a completely different interpretation, based on the fact that the crystal growth is homothetic, i.e., it involves uniform expansion or contraction of the interface. Essentially, what is achieved in all models based on the Frank's equation is that an infinitely narrow (i.e., sharp) moving interface is used to represent a solid-liquid boundary over which conditions of temperature and composition must be satisfied. Because of the discrete sharp boundary, mathematical singularity was encountered. The solution therefore did not allow a true velocity selection, but only allowed for obtaining a steady state solution for a range of velocities [24]. Surface topology of single crystals continues to attract the interest of the polymer community. One of the latest attempts was due to Hu *et al*. [25] who have demonstrated, based on the Monte Carlo simulations, the growth of shish-kebab structures growing during polymer crystallization. Although the simulated shish-kebab structure was similar to the experimental one, the origin of the emerged periodicity was not addressed.

In 1937, Landau [26] developed a theory of phase transition, where he represented the phase in the form of a continuous field of an order parameter ψ, which has different stable values in different phases. Landau expressed the free energy of phase transition in the form of an expansion in powers of the order parameter, $\Delta f = A\psi^2 + B\psi^3 + C\psi^4 + \cdots$. The first-order term of the expansion is always zero so that the free energy is invariant in all coordinate transformation. The coefficients of the second-, third-, and fourth-order terms A, B, and C, are recognized as functions of such variables as pressure and temperature. Landau specified the conditions for first-and second-order transition: for a second-order transition the coefficient of third-order B is exactly zero; for the first-order, B is nonzero. In the former case, the free energy is symmetric double well and the chemical potential has two roots that differ only in sign. In the latter case, the free energy is an asymmetric double well, which accounts for the metastability. A time dependent form of this theory, also called a time dependent Ginzburg-Landau (TDGL) theory, was applied explicitly to the first-order phase transition by Chan [27]. He showed that the unique characteristics of the first-order phase transitions, viz., the presence of a rather sharp interface and latent heat of phase transitions can be recovered from the solution of such a model.

In a previous paper [28], we proposed a phase field model [29,30] based on a nonconserved time dependent Ginzburg-Landau (TDGL model *A*) equation, which expressed the entire system as a time dependent spatial field of a scalar order parameter, undergoing phase transitions from amorphous melt to crystalline solid. The uniqueness of the model is the diffuse interface that eliminates the numerical singularity inherent in the original Frank's equation. This approach was originally applied to describe the crystallization of metallic crystals [29,30]. Recently, it has been extended by us for the elucidation of both diamond-shaped and curved polyethylene single crystals [28]. However, the above TDGL model *A* equation alone is incapable of generating the ripples observed experimentally in sPP. This has led to the present study in which we adopt two coupled nonlinear reaction diffusion equations to demonstrate possible influence of mechanical coupling on the corrugated ripple textures in sPP single crystals subjected to quiescent isothermal crystallization.

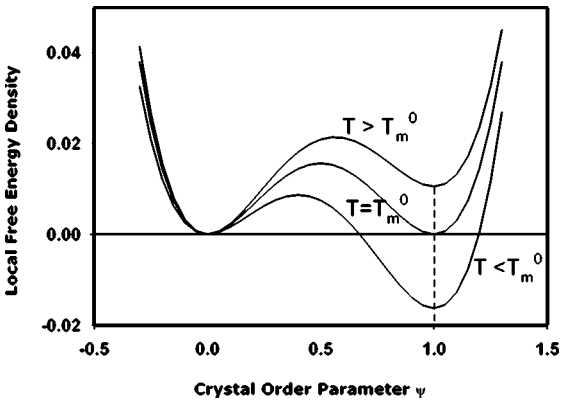

FIG. 1. Schematic plot of local free energy density and crystal order parameter ψ for various temperatures showing the metastable energy barrier for phase transition from the melt ($\psi=0$) to the crystalline state ($\psi=1$). At equilibrium melting point at T_m^0 the free energy level of both the melt and crystalline state is the same.

II. THEORETICAL SCHEME

The total free energy of crystal ordering may be described by

$$F = \int (f_{local} + f_{grad}) d\Omega, \tag{1}$$

where the free energy density of crystal ordering consists of a local term and a nonlocal gradient term. The f_{local} is given in the form of Landau expansion of a nonconserved crystal order parameter, ψ [30,31], viz.,

$$f_{local}(\psi) = W_{\psi} \int_0^{\psi} p(p-1)(p-\zeta)\, dp = W^{\psi}\left[\zeta\frac{\psi^2}{2} - (1+\zeta)\frac{\psi^3}{3} + \frac{\psi^4}{4}\right]. \tag{2}$$

This local free energy has an asymmetric double well potential for crystal ordering with respect to ψ, in which $\psi=1$ represents the crystalline solid, whereas $\psi=0$ represents the amorphous melt (Fig. 1). W^{ψ} is a dimensionless constant representing the strength of the potential field pertaining to ψ, and ζ represents the peak position of the energy barrier.

The nonlocal free energy term f_{grad} is customarily given as

$$f_{grad}(\psi) = \frac{(\boldsymbol{\kappa}^{\psi} \cdot \nabla \psi)^2}{2}, \tag{3}$$

where $\boldsymbol{\kappa}^{\psi}$ is the tensor representing the coefficient of the interface gradients of the ψ field, the dot product of $\boldsymbol{\kappa}^{\psi}$ and $\nabla\psi$ is vector, and thus its square is scalar. Note that the

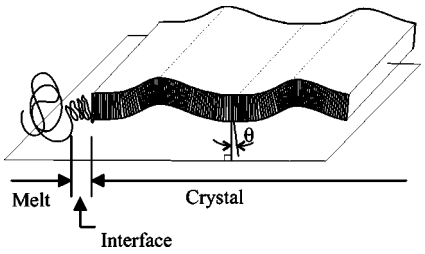

FIG. 2. Schematic sketch displaying a chain folded lamella with periodic undulations, in which chain tilting occurs, represented by a tilt angle θ made by the chain stem with the normal to the plane of the lamella together with the solid-liquid interface having an intermediate degree of order.

interface gradient free energy is nonzero only at the interface $(0<\psi<1)$.

Although the polymer chains are flexible in the melt, these molecules become significantly stiffer upon incorporating into the crystals. However, the crystal-melt interface behaves like liquid crystals or liquid membranes of colloidal systems having intermediate properties between the liquid and solid polymer single crystal. To appreciate such a picture, a schematic sketch displaying a chain folded lamella with periodic undulations is shown in Fig. 2, in which chain tilting occurs, which is represented by a tilt angle θ made by the chain stem with the normal to the average plane of the lamella. Polymer crystal is a planar ensemble of chain stems standing parallel to each other. Thus, any out of plane chain tilting imposes a curvature elastic free energy penalty. Since the solid-liquid interface has an intermediate degree of order, it is necessary to take into consideration a higher order curvature elastic term to reflect the crystal-melt interface. We define the chain-tilting angle θ as the angle made by the polymer chain stems with the normal to the average plane of lamella (Fig. 2). Then the curvature elastic free energy can be expressed as:

$$f_{ce} = \tfrac{1}{2}[\kappa^{\theta}(\nabla\theta)^2 + \varepsilon(\nabla^2\theta)^2], \tag{4}$$

where κ^{θ} and ε are coefficients of the gradients of θ field, representing the second-order and fourth-order curvature elastic terms, respectively. Physically, the first term in Eq. (4) denotes the nonlocal free energy arising from the gradient of the interface associated with tension, whereas the second term refers to nonlocal free energy due to the curvature elasticity due to bending. The detailed derivation of this free energy may be found in Guenthner and Kyu [32].

This chain tilting process was originally introduced to describe the development of banded textures in liquid crystalline polymers after cessation of shear [32], in which the emergence of banded textures in the liquid crystalline polymers has been explained satisfactorily. When the crystallization is taking place, there is a stress built up at the interface. One mean of releasing the stress is through a relaxation process, which may occur in the form of local reorientation such as the chain tilting. Assuming that the deformation is small, the strain in the melt at the interface may be given as

$$\frac{\lambda}{\lambda_r} = \cos\,\theta, \tag{5}$$

where λ_r is the maximum recoverable strain in the material, and θ is the chain tilt angle. Using a neo-Hookean-type potential, the free energy density of elastic deformation may be written as

$$f_{el} = W^{\theta}[(\lambda_r\cos\,\theta)^2 + 1/(\lambda_r\cos\,\theta)^2 - 2], \tag{6}$$

where W^{θ} is the elastic modulus. For small deformation strains we have $\cos\,\theta \approx 1-\theta^2/2$ and $1/\cos\,\theta \approx 1+\theta^2/2$. If the chain tilt angle θ is small then the recoverable strain must also be small, i.e., defing the variable $\varphi = 4(\lambda_r - 1)$, φ must also be small. Neglecting higher powers of φ we can write $\lambda_r^2 = (1+\varphi/4)^2 \approx 1+\varphi/2$, and $1/\lambda_r^2 \approx (1-\varphi/4)^2 \approx 1-\varphi/2$. Substituting these apporximations in Eq. (6), one obtains

$$f_{el} = W^{\theta}\left[\frac{\theta^4}{2} - 4(\lambda_r - 1)\theta^2\right]. \tag{7}$$

Physically Eq. (7) represents the strain recovery potential associated with the deformation or volume contraction during crystallization. This free energy has two minima at $\pm\varphi^{1/2} = \pm 2\sqrt{(\lambda_r - 1)}$, representing the two stable orientations. The ordering in the orientational field takes place in conjunction with the propagation of the interface in the crystal order parameter field. Since the two order parameter fields do not occur independently during crystallization, these two processes must be coupled through a term composed of a linear and/or quadratic dependence of order parameters as follow:

$$f_{couple} = -\alpha\theta(\psi - \psi^2), \tag{8}$$

α is the coupling strength, which is normally weak, i.e., $\alpha \ll W^{\psi}$. This coupling term was chosen to be nonsymmetric in θ, so that the system can discriminate the chain tilting in one sector from that in the other sector in the crystal.

The total free energy functional, $F(\psi)$ is then given as

$$F(\psi) = \int W^{\psi}\left[\zeta\frac{\psi^2}{2} - (1+\zeta)\frac{\psi^3}{3} + \frac{\psi^4}{4}\right] + \frac{(\boldsymbol{\kappa}^{\psi}\cdot\nabla\psi)^2}{2} + \frac{1}{2}\left\{\kappa^{\theta}(\nabla\theta)^2 + \varepsilon(\nabla^2\theta)^2 + W^{\theta}\left[\frac{\theta^4}{2} - 4(\lambda_r - 1)\theta^2\right]\right\} - \alpha\theta(\psi - \psi^2)d\Omega. \tag{9}$$

The total free energy of Eq. (9) is further inserted in two nonconserved TDGL equations, viz., $\partial\psi/\partial t = -\Gamma^{\psi}\delta F/\delta\psi$ and $\partial\theta/\partial t = -\Gamma^{\theta}\delta F/\delta\theta$, to give

$$\frac{\partial\psi}{\partial t} = -\Gamma^{\psi}[W^{\psi}\psi(\psi-1)(\psi-\zeta) - (\kappa^{\psi})^2\nabla^2\psi + \alpha\theta(1-2\psi)], \tag{10}$$

$$\frac{\partial\theta}{\partial t} = -\Gamma^{\theta}\{W^{\theta}\theta[4(\lambda_r - 1) - \theta^2] - \kappa^{\theta}\nabla^2\theta + \varepsilon\nabla^4\theta + \alpha\psi(1-\psi)\}, \tag{11}$$

where Γ^{ψ} is the mobility representing the propagation of the

interface that is inversely proportional to the viscosity or the frictional coefficient, whereas Γ^{θ} is the rotational mobility associated with the orientation of the chain in the dissipative medium. Physically, Eq. (10) signifies the spatio-temporal evolution of crystal order parameter [28], whereas Eq. (11) arises due to the strain recovery deformation.

It may be noted here that the coupling term, $\alpha\psi(1-\psi)$ in Eq. (11) is nonzero only at the interface and therefore induced deformation must occur at the interface. On the other hand, the coupling term, $\alpha\theta(1-2\psi)$ in Eq. (10) promotes crystallization in regions that simultaneously deform to accommodate the coupling effect. It is apparent that the $\alpha\theta(1-2\psi)$ term changes its sign during crystallization, i.e., it is positive in the melt ($\psi<1/2$) and becomes negative when it is in the crystalline state ($\psi>1/2$). During crystallization at the interface where $\psi>1/2$ the coupling terms in the ψ and θ have opposite signs. Therefore, the two propagating waves mutually interfere during solidification, resulting in the transformation from the solitary wave to the oscillatory wave, which in turn generates a rich variety of morphological patterns. If the coupling terms in the two equations have the same sign, the two waves propagate in the same direction without any interference. As a consequence, there will be no pattern formation. Hence the opposite sign of the coupling terms in the two corresponding fields is the essential criterion in order to discern any pattern formation. It should be emphasized that a simple linear or quadratic coupling in the two model *A* equations will not generate any patterns.

Using D as the diffusion constant and d^{*} as the characteristic length, we can convert Eqs. (10) and (11) into the nondimensionless form

$$\frac{\partial \psi}{\partial \tau} = -\tilde{\Gamma}^{\psi}[W^{\psi}\psi(\psi-1)(\psi-\zeta) - (\tilde{\kappa}^{\psi})^2\nabla^2\psi + \alpha\theta(1-2\psi)], \tag{12}$$

$$\frac{\partial \theta}{\partial \tau} = -\tilde{\Gamma}^{\theta}\{W^{\theta}\theta[4(\lambda_r-1)-\theta^2] - \tilde{\kappa}^{\theta}\nabla^2\theta + \tilde{\varepsilon}\nabla^4\theta + \alpha\psi(1-\psi)\}, \tag{13}$$

where,

$$\tau=\frac{D}{d^{*2}}t, \tilde{\mathrm{x}}^2 = \frac{\mathrm{x}^2}{d^{*2}}, \quad \tilde{\Gamma}^{\psi} = \Gamma^{\psi}\frac{d^{*2}}{D}, \quad \tilde{\Gamma}^{\theta} = \Gamma^{\theta}\frac{d^{*2}}{D},$$
$$(\tilde{\kappa}^{\psi})^2 = \frac{(\kappa^{\psi})^2}{d^{*2}}, \quad \tilde{\kappa}^{\theta} = \frac{\kappa^{\theta}}{d^{*}}, \quad \tilde{\varepsilon} = \frac{\varepsilon}{d^{*4}}. \tag{14}$$

It should be pointed out that except for the coupling coefficient α there is no adjustable parameter in Eq. (12); that is to say, all the remaining model parameters can be determined experimentally (see the Appendix). However, there is no experimental means of determining the parameters in the governing equation [Eq. (13)].

Equation (12) and (13) were solved numerically in two dimensions on a square lattice (256×256) using central finite forward difference scheme for spatial discretization and explicit forward difference for time steps with an absorbing boundary condition. The simulation was performed using various temporal steps ($\Delta\tau$) on several grids (64×64, 128×128, 256×256, 512×512, and 1024×1024) to assure the stability of the simulation; however, only the results of (512×512) simulation are shown here. To avoid over crowding only a single nucleus was triggered via perturbation in the simulation.

III. RESULTS AND DISCUSSION

The uniqueness of the phase field approach is the double well potential that is capable of describing the metastability inherent to crystallization. Here, the double well potential has been mathematically described in the framework of a Landau type free energy expansion by use of a crystal order parameter ψ [31]. The free energy double well has been optimized to the experimental conditions involving crystallization temperature, and material properties of the polymer (i.e., sPP) such as the apparent melting point at that specific crystallization temperature, the equilibrium melting point, and the latent heat of crystallization of the sPP (see the Appendix). The higher of the two minima in the free energy represents the metastable state whereas the lower minimum represents a more stable solid state. It should be emphasized that this free energy state at $\psi=1$ is not necessarily equal to the final equilibrium state, but it merely corresponds to that of the lamellar thickness l_z that a crystal achieves at a given crystallization temperature, because the crystal order parameter has been normalized as $\psi=l/l_z$. It is plausible that polymer crystallization possesses many levels of metastability, as crystallizing chains may not necessarily achieve a true equilibrium state. Although the polymer crystals may be trapped kinetically in a metastable state, it is nonetheless more stable than the melt [33,34]. Even if the present double well is replaced by multiple well, the intermediate metastable states, if present, are short lived when compared to the time scale under consideration, especially in the context of the coarse grain model being considered here. In addition, only two states, metastable or otherwise, i.e., the melt and crystalline states, have been predominantly observed during the course of crystallization; unless the short-lived intermediate metastable states have been deliberately trapped by some experimental means. Hence, the current double well approach of Fig. 1 should be adequate for the description of the traditional isothermal crystallization. However, if one chooses to explain the entrapped metastable states, the current phase field approach may be modified with multiple-well potentials, which is evidently beyond the scope of this work.

In a recent optical microscopic investigation of a blend of syndiotactic polypropylene (sPP) and poly (ethylene octene) copolymer (POE) isothermally crystallized at 120°C from the melt (160°C), a rectangular shaped crystal grows into a sizable single crystal that can be discerned under optical microscope [35]. As depicted in Fig. 3, the tiny periodic striations appear running across the long axis of the single crystal. Although the crystallization was carried out from the melt, it is conceptually similar to the solution crystallization because POE effectively acts like a polymer diluent to sPP. The atomic force microscopic investigation was undertaken

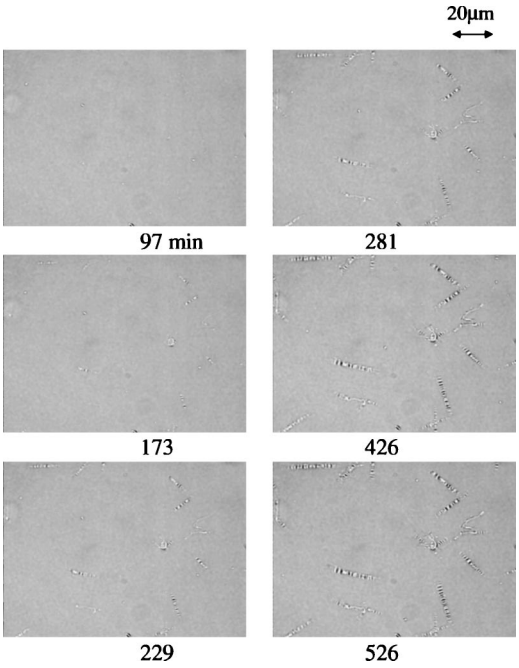

FIG. 3. Optical microscope micrograph showing the spatio-temporal evolution of ripples in a single crystal of syndiotactic polypropylene in 30/70 melt blend of sPP and poly (ethylene octene) copolymer following isothermal crystallization at 120°C quenched from 160°C. These pictures were obtained using an Olympus optical microscope, model BX 60.

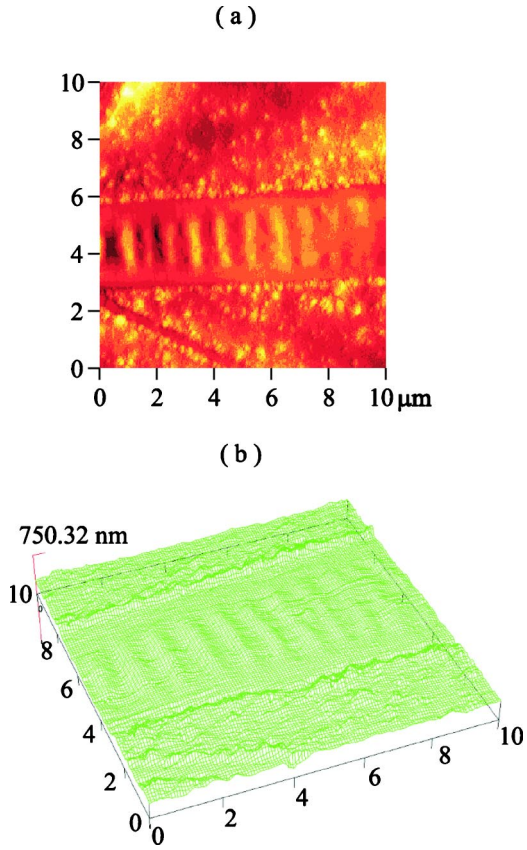

FIG. 4. Atomic force microscope micrograph showing the emergence of ripples in a single crystal of syndiotactic polypropylene in 2/98 melt blend of sPP and poly (ethylene octene) copolymer following isothermal crystallization at 120°C quenched from 160°C. These images were obtained using Quesant atomic force microscope (AFM), model Q-SCOPE 350: (a) wave mode and (b) the corresponding contour plot. The scale was 2 μm per division.

to identify these periodic ripples, which turned out to be the corrugated ridges [Fig. 4(a)] similar to those reported by others [1,9], except that these ridges primarily formed in the middle section of the sPP single crystal. It should be emphasized that the present optical micrograph was taken at the crystallization temperature (120°C); thus, these periodic ridges emerge *in situ* during the course of crystallization, and thus discounting earlier explanation of thermal contraction of the single crystal upon cooling [6]. The contour map of the atomic force micrograph shows clearly that these periodic ridges are confined to thin sectors of the fastest growing front [Fig. 4(b)]. This observation gives a hint that some types of mechanical deformation might have occurred in the aforementioned anisotropic crystallization, thereby influencing the morphology of single crystals. Physically, the polymer melt is highly constrained along the fastest growing *b*-axis direction. When the crystallization takes place following thermal quenching, there is a sudden increase in density of the emerging crystals, which in turn makes the volume of the constrained melt to shrink at the solid-liquid interface (i.e., crystallizing front) (Fig. 2). If the shrinkage takes place preferentially along the constrained direction, one possible scenario in releasing the internal stress is through formation of periodic ripples as the propagating lamellar front solidifies. If the lateral shrinkage occurs, a mechanical torque would develop causing the emerging lamella to twist although the crystallization is supposedly under quiescent conditions.

In the absence of the stress, the system reduces to Eq. (12) which is essentialy the TDGL (model *A*) pertaining to the nonconserved crystal order parameter ψ. This model *A* has been successfully applied to predicting various crystal topologies such as faceted and curved single crystals [28]. The first term on the right hand side of Eq. (12) is due to the surface nucleation, whereas the second term represents the interface propagation signifying the growth. The general treatement given by the existing nucleation theories for polymer crystallization gives the structure formed at the asymptotic equilibrium through minimization of the free energy with respect to the lamellar thickness. The classical kinetic equation therefore represents only the velocity of crystal growth. Since the original LH theory lacks the spatial diffusive term, Mansfield [21] employed the Frank's theory, which involves the first-order moving boundary equation to account for the spatio-temporal growth. The solution of the Frank's equation encountered mathematical singularity because of the sharp interface of zero thickness. This sharp boundary problem could have been avoided, had the time-dependent second-order diffusion equation of the BCF theory been adopted instead [12]. The advantage of the BCF theory is that the crystal interface is relatively smooth, similar to what we have been advocating in the present theoretical work. One advantage of the present phase field model is

TABLE I. Model parameters calculated from experimentally determined material parameters of sPP at a given experimental temperature.

(a) Material parameters		(b) Model Parameters	
ΔH_u [a]	1.714×10^{8} J/m^3	Γ^{ψ}	4.875×10^{-2} s^{-1}
ν	10^{8} m/s	$(\kappa^{\psi})^2_{11}$	3.872×10^{-16} m^2
σ_{av} [b]	0.0109 J/m^2	$(\kappa^{\psi})^2_{22}$	6.491×10^{-16} m^2
σ_{11} [c]	0.0096 J/m^2	W^{ψ}	3409
σ_{22} [d]	0.01243 J/m^2	ζ	0.3431
T_m^0 [e]	434 K		
T_m	413 K		
T	398 K		

[a]Reference [43].
[b]$\sigma_{av}=0.1\sqrt{ab}\Delta H_u$ as in Ref. [44], where a and b are crystallographic dimensions.
[c]$\sigma_{11}=0.1b\Delta H_u$.
[d]$\sigma_{11}=0.1a\Delta H_u$.
[e]Reference [45].

that the asymmetric potential was used in the ψ field to account for the metastability for nucleation. If one utilizes a single well potential, $f_{local}\propto\psi^2$ in Eq. (2), the BCF equation can be recovered, which predicts the structure at equilibrium. However, the single well potential is incapable of explaining the metastability, which is an essential part of polymer crystallization.

It should be emphasized that a single equation alone is inadequate for explaining the intricate morphological textures of lamellar crystals such as sectorized single crystals, corrugated ripples, among others. Sectorization is a ubiquitous feature observed in polymer single crystals, which is thought to be a result of the fact that orientation of the folds varies from region to region within the same single crystal. In other words, a single crystal is thus divided into a fixed number of regions called sectors such that the orientation of the folds on the surface within a given sector is uniform [36]. The existence of sectors in single crystals of syndiotactic polypropylene [37] and polyethylene [38] has been directly confirmed in the investigation by atomic force microscopy. A question arises as to the significance of these sector demarcations that appeared in the final morphological images.

In order to investigate the origin of the sector demarcation in the single crystals using the model proposed above, numerical simulation was carried out based on the values of various dimensionless coefficients of Eq. (12) [Table I(b)], calculated from various experimentally derivable properties of sPP listed in Table I(a). In the absence of the deformation term, $f_{el}=0$, the sectorization in the emerging single crystals was captured theoretically for the first time in both the order parameter and the tilt-angle fields (see Fig. 5), although these sectorized single crystals, having two sectors along the fast growing front and the remaining two along the slow growing front, have long been recognized experimentally [1,9]. As the single crystal comprises plate-like sectors, it is possible that these plates would have a small variation in their overall orientation arising from their curvature elastic term, i.e., $\tilde{\varepsilon}\nabla^4\theta$. It is apparent that boundaries demarcating these sectors are simply the trajectories of the growth that run diagonally between the (010) and (100) directions from the common nucleus. These trajectories are the demarcation of polymer chains having different chain orientations (or tilt angles). It should be emphasized that these sectorized boundaries could be recorded permanently only when the fourth-order derivative curvature elastic term was included in the simulation, thereby signifying the role of the curvature elasticity in the formation of these sectors.

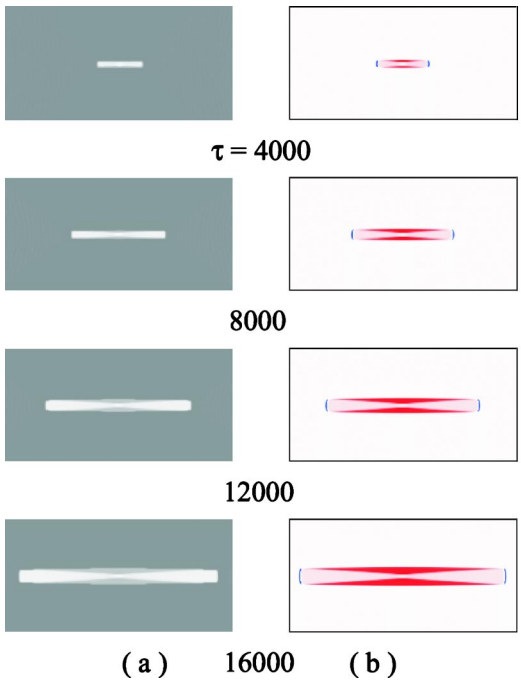

FIG. 5. Spatio-temporal growth of syndiotactic polypropylene single crystals, exhibiting sectorization as simulated based on the coupled Eqs. (12) and (13) using the experimentally determined material parameters listed in Table I(b) and $\tilde{\Gamma}^{\theta}=0.4$, $\tilde{\kappa}^{\theta}=0$, $\tilde{\varepsilon}=0.3$, and $\alpha=0.1$. (a) the crystal order parameter ψ, (b) the tilt angle θ.

As pointed earlier, the shrinkage of the constrained melt can cause the internal stress to develop at the solid-liquid interface by virtue of a sudden increase in density in the crystalline phase. To release the stress, the emerging lamella may buckle as the uniaxial shrinkage occurs in the b-axis direction or may twist in the case of lateral contraction. When the stress relaxes slowly due to high viscosity of the polymer melt at the interface, the lamellar single crystal has to deform as a means of releasing the excess stress. The question is why the lamellar single crystal has to deform in a periodic manner. A possible account is due to the induced mechanical field during isothermal crystallization.

We therefore attempted to couple the two nonlinear processes of crystallization and mechanical deformation in order to explain the unique morphology observed in case of sPP single crystal. As expected, the solution of the coupled Eqs. (12) and (13), gives the oscillatory wave propagation leading to emergence of periodic texture. The initial nucleus is isotropic (picture not shown), but the emerging single crystal becomes anisotropic with elapsed time by virtue of the difference in the growth habits of sPP in which the directional growth in the b-axis direction is faster than that along the a

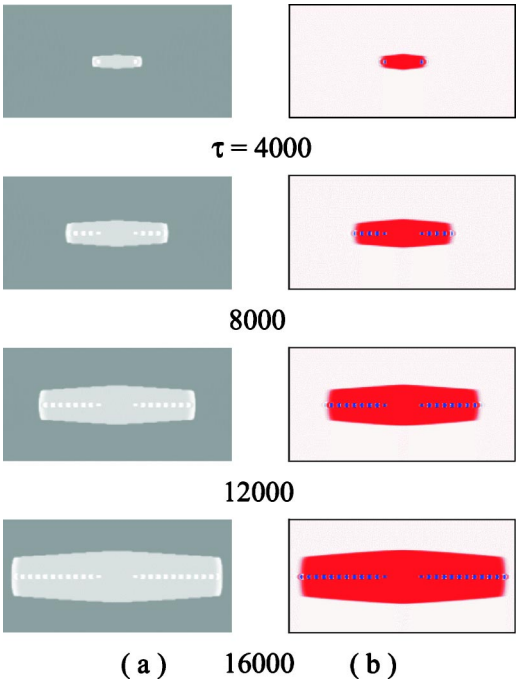

FIG. 6. Spatio-temporal growth of syndiotactic polypropylene single crystals, exhibiting ripple formation in the sectors belonging to the long axis in both fields: (a) the crystal order parameter and (b) the tilt angle. The simulation was carried using the experimentally determined materials parameters of Table I (b) along with $\tilde{\Gamma}^{\theta}=0.4$, $\tilde{\kappa}^{\theta}=0$, $\tilde{\varepsilon}=0.3$, and $\alpha=0.1$.

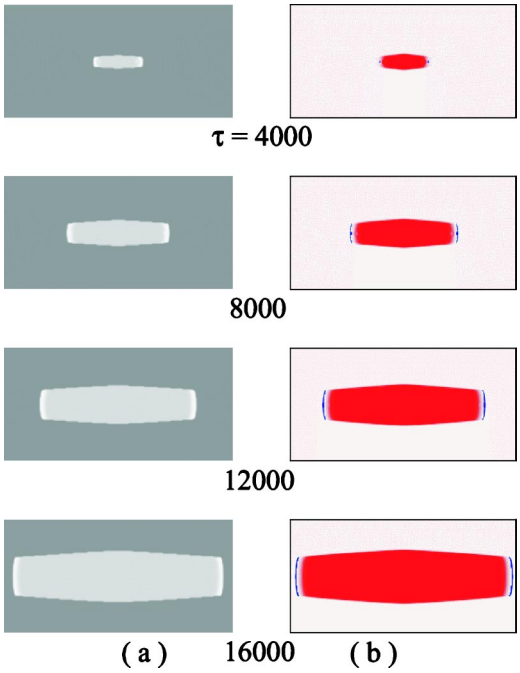

FIG. 7. Spatio-temporal growth of syndiotactic polypropylene single crystals, with the coefficient of curvature elasticity $\tilde{\varepsilon}$ below a critical value of 0.26, exhibiting ripple formation which is washed away as the crystal grows: (a) the crystal order parameter ψ and (b) the tilt angle θ. The simulation was carried using the experimentally determined materials parameters of Table I(b) along with $\tilde{\Gamma}^{\theta}=0.4$, $\tilde{\kappa}^{\theta}=0$, $\tilde{\varepsilon}=0.25$, and $\alpha=0.1$.

axis, reflecting the differential fold energies along the two growth fronts [5]. Concurrently, the periodic ripples form in the emerging single crystal, predominantly in the sectors that belong to the long single crystal axis (Fig. 6). It is striking that the simulated periodic pattern is in close agreement with that observed experimentally by us for sPP (Fig. 3), although it is not our primary intention to match with any particular set of experimental results. Although presently it may not be feasible to experimentally determine the dimensionless parameter $\tilde{\varepsilon}$ in Eq. (13), it may be instructive to demonstrate the effect of $\tilde{\varepsilon}$ on the length scale such as lamellar crystal size and periodicity of the ripples, as well as their shapes. In absence of the higher order curvature gradient term $\tilde{\varepsilon}$ or when its value falls below the critical value of $\tilde{\varepsilon}$, the ripples disappear (Fig. 7). This behavior is consistent with the theoretical demonstration by Guenthner and Kyu [32] that the propagation of the domain wall (solitary wave) can transform into the oscillatory wave when the coefficient of the curvature gradient $\tilde{\varepsilon}$ exceeds the critical value, and vice versa.

It is noticed that there are some differences between the experiments of Lovinger *et al.* [6] and the present study. That is to say, their periodic ripples are located in the thick transverse sectors of the sPP single crystals [6] as opposed to our finding in which the periodic ridges are confined to the thin sectors along the long lamellar axis. Another difference is the crystallization condition, in which crystallization was carried out in the neat sPP from the melt in Lovinger's case as opposed to the crystallization in the miscible blends of sPP/POE (i.e., POE acts like a polymeric solvent to sPP) in the present study. Although our observation in sPP is in good accord with those of the solution grown PE by Basset and Keller [9], the two seemingly different findings of Lovinger *et al.* [6] and ours can be reconciled by merely decreasing the strength of the coupling through α. This leads to a more restricted faceted growth leading to stress concentration in both thin and thick sectors. As evidenced in Fig. 8, the simulated pattern with a lower coefficient of coupling term indeed shows the formation of the periodic ripples in both thin and thick sectors of the lamellar single crystals, which in turn confirms that both experimental observations by Lovinger *et al.* and ours are not necessarily contradictory, but rather complimentary to each other.

IV. CONCLUSIONS

In summary, the present theory gives a more comprehensive description of polymer crystallization relative to the BCF or the Mansfield's theory. This paper clearly demonstrates the profound influence of the self-generated mechanical fields such as curvature elasticity and strain recovery deformation on the intricate morphological textures of polymer single crystals. It becomes apparent that the higher order curvature elasticity is crucial to discern the sectorization and ripple formation in the polymer single crystals. The sectorized boundaries are simply the trajectories of the resultant growth direction that demarcate the regions of different chain orientations (or tilt angles). The coupling between the crys-

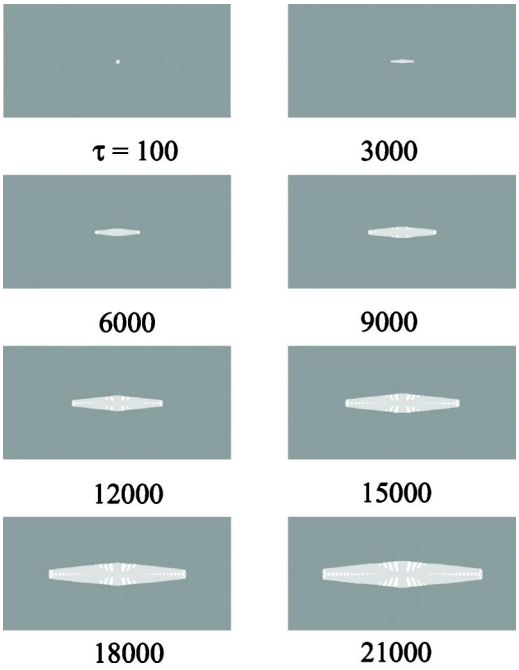

FIG. 8. Anisotropic single crystal showing ripple formation in all four sectors as seen in the crystal order parameter field ψ with the experimentally determined materials parameters listed in Table I(b) in conjunction with $\tilde{\Gamma}^{\theta}=0.4$, $\tilde{\varepsilon}=0.3$, $\tilde{\kappa}^{\theta}=0$, and $\alpha=0.025$.

tallization and strain recovery deformation further captured the corrugated ripple textures in both thin and thick sectors of the single crystal. More importantly, these predicted topologies have been observed experimentally in the melt crystallized single crystals of syndiotactic polypropylene (at least by us) as well as in the solution grown polyethylene. Although the possible involvement of the mechanical deformation has long been suspected to exert some influence on the quiescent polymer crystallization, the present theoretical calculation is the first to demonstrate the need for taking into consideration the induced mechanical field in explaining intricate single crystal morphology.

ACKNOWLEDGMENT

Support of this work by Grants Nos. NSF-DMR 99-03519, DMR 02-09272, and Ohio Board of Regent Research Challenge Grant is gratefully acknowledged.

APPENDIX: RELATIONSHIP BETWEEN MODEL PARAMETERS AND CLASSICAL MATERIAL PARAMETERES

Model parameters in Eq. (10) can be related to experimental conditions and/or classical material properties that are characteristics to the polymer under consideration. According to Eq. (2) the change in the local free energy due to crystallization is given as

$$\Delta f_{local}(\psi) = \frac{W^{\psi}}{6}[\zeta - 1/2]. \tag{A1}$$

For a crystal of average thickness l and having a cross-sectional area A, the Gibbs free energy is given as

$$\Delta f_{local} = 2A\sigma_e - Al\Delta H_u(1 - T/T_m^0), \tag{A2}$$

where T is the crystallization temperature and T_m^0 is the equilibrium melting temperature of the polymer. σ_e is the surface free energy per unit area of the folded surface and ΔH_u is the latent heat of crystallization. This free energy per unit volume occupied by a stem may be expressed as

$$\frac{\Delta f_{local}}{Al_z} = 2\frac{\sigma_e}{l_z} - \Delta H_u(1 - T/T_m^0)\psi, \tag{A3}$$

where $\psi = l/l_z$, and l_z is the stable lamellar thickness of the crystal. At the crystallization temperature T the free energy Δf_{local} is zero when a critical lamellar thickness l^* is reached:

$$2\frac{\sigma_e}{l^*} - \Delta H_u(1 - T/T_m^0) = 0. \tag{A4}$$

By using the Hoffman and Weeks relationship [39], the melting temperature T_m of the crystal is related to its lamellar thickness l_z:

$$2\frac{\sigma_e}{l_z} - \Delta H_u(1 - T_m/T_m^0) = 0. \tag{A5}$$

Using Eqs. (A4) and (A5) we can obtain the critical order parameter for which $\Delta f_{local}=0$:

$$\psi^* = \frac{l^*}{l_z} = \frac{T_m^0 - T_m}{T_m^0 - T}. \tag{A6}$$

From Eq. (2) one can relate the peak position of the energy barrier ζ to the stability order parameter ψ^*:

$$\zeta = \frac{4\psi^* - 3\psi^{*2}}{6 - 4\psi^*}. \tag{A7}$$

The excess free energy at the interface (or the surface) energy σ may be evaluated in accordance with Cahn and co-workers' approach [40,41], i.e.,

$$\frac{\sigma}{nRT} = \int_0^1 \kappa^{\psi}\sqrt{2f_{local}}\, d\psi. \tag{A8}$$

At $T=T_m$ the surface energy is given from the Eq. (A8) and using Eq. (2) as

$$\frac{\sigma}{nRT} = \frac{\kappa^{\psi}}{6}(W^{\psi}/2)^{1/2}. \tag{A9}$$

Therefore,

$$\kappa^{\psi} = 6(2/W^{\psi})^{1/2}\frac{\sigma}{nRT}. \tag{A10}$$

Further, the interfacial thickness δ is estimated as

$$\delta = \kappa^{\psi}\sqrt{1/(2f_{local\ \max})}. \tag{A11}$$

Using Eq. (2) we obtain

$$\delta = 4\kappa^{\psi}(2/W^{\psi})^{1/2}. \tag{A12}$$

According to Harrowell and Oxtoby [42], Γ can be related to the velocity v of the interface as follows:

$$v = -\frac{3}{2\sqrt{2}}\Gamma\delta\Delta f_{local}. \tag{A13}$$

Using Eqs. (2), (A10), and (A12) we obtain the relationship

$$\Gamma^{\psi} = \frac{\sqrt{2}}{12}v\left[\frac{\sigma}{nRT}(1/2-\zeta)\right]^{-1}. \tag{A14}$$

[1] P. H. Geil, *Polymer Single Crystals* (Krieger, Huntington, NY, 1973).
[2] F. Khoury and E. Passaglia, in *Treatise On Solid-State Chemistry*, edited by N. B. Hannay (Plenum Press, New York, 1976), Vol. 3, p. 335.
[3] D. C. Bassett, *Principles Of Polymer Morphology* (Cambridge University Press, New York, 1981).
[4] G. Stroble, *The Physics Of Polymer* (Springer-Verlag, Berlin, 1996).
[5] B. Lotz, A. J. Lovinger, and R. E. Cais, Macromolecules **21**, 2375 (1988).
[6] A. Lovinger, B. Lotz, D. D. Davis, and M. Schumacher, Macromolecules **27**, 6603 (1994).
[7] V. V. Tsukruk and D. H. Reneker, Phys. Rev. B **51**, 6089 (1995).
[8] V. V. Tsukruk and D. H. Reneker, Macromolecules **28**, 1370 (1995).
[9] D. C. Bassett and A. Keller, Philos. Mag. **6**, 345 (1961); Ref. [1], p. 94 and p. 138.
[10] N. Cabrera and W. K. Burton, Discuss. Faraday Soc. **5**, 33 (1949); **5**, 40 (1949).
[11] W. K. Burton, N. Cabrera, and F. C. Frank, Philos. Trans. R. Soc. London, Ser. A **243**, 299 (1951).
[12] A. Pimpinelli and J. Villain, *Physics of Crystal Growth* (Cambridge University Press, Cambridge, 1998), p. 89.
[13] J. I. Lauritzen and J. D. Hoffman, J. Chem. Phys. **31**, 1680 (1959); J. Res. Natl. Bur. Stand., Sect. A **65**, 297 (1961).
[14] J. D. Hoffman, G. T. Davis, and J. L. Lauritzen, Jr., in *Treatise On Solid-State Chemistry*, edited by N. B. Hannay (Plenum Press, New York, 1976), Vol. 3, p. 497.
[15] M. Muthukumar and P. Welch, Polymer **41**, 8833 (2000).
[16] P. Welch and M. Muthukumar, Phys. Rev. Lett. **87**, 218302 (2001).
[17] J. D. Hoffman and R. L. Miller, Macromolecules **22**, 3038 (1989).
[18] R. L. Miller and J. D. Hoffman, Polymer **32**, 963 (1991).
[19] D. M. Sadler, Polymer **24**, 1401 (1983); **28**, 1440 (1987).
[20] D. M. Sadler and G. H. Gilmer, Polymer **25**, 1446 (1984).
[21] M. L. Mansfield, Polym. Commun. **29**, 1755 (1988); Polymer **31**, 283 (1990).
[22] F. C. Frank, J. Cryst. Growth **22**, 233 (1974).
[23] J.-J. Point and D. Villers, Polymer **33**, 2263 (1992).
[24] S. A. Schofield and D. W. Oxtoby, J. Chem. Phys. **94**, 2176 (1991).
[25] W. Hu, D. Frenkel, and V. B. F. Mathot, Macromolecules **35**, 7172 (2002).
[26] L. D. Landau, Zh. Eksp. Teor. Fiz. **7**, 19 (1937); **7**, 637 (1937). [English translations in *Collected Papers of L. D. Landau*, edited by D. Ter Haar (Gordon and Breach, New York, 1965), pp. 193, 209].
[27] S.-K. Chan, J. Chem. Phys. **67**, 5755 (1977).
[28] T. Kyu, R. Mehta, and H.-W. Chiu, Phys. Rev. E **61**, 4161 (2000).
[29] G. Caginalp and E. A. Sokolovsky, Appl. Math. Lett. **2**, 117 (1989).
[30] A. A. Wheeler, W. J. Boettinger, and G. B. McFadden, Phys. Rev. A **45**, 7424 (1992).
[31] R. Kobayashi, Physica D **63**, 410 (1993).
[32] A. J. Guenthner and T. Kyu, Macromolecules **33**, 4463 (2000).
[33] P. H. Lindenmeyer, J. Chem. Phys. **46**, 1902 (1967); J. Polym. Sci., Part C: Polym. Symp. **20**, 145 (1967).
[34] P. H. Lindenmeyer and J. M. Peterson, J. Appl. Phys. **39**, 4929 (1968).
[35] W. Keawwattana, PhD Dissertation (The University of Akron, Akron, OH, 2002).
[36] D. H. Reneker and P. H. Geil, J. Appl. Phys. **31**, 1916 (1960).
[37] W. Zhou, S. Z. D. Cheng, S. Putthanarat, R. K. Eby, D. H. Reneker, B. Lotz, S. Magonov, E. T. Hsieh, R. G. Geerts, S. J. Palackal, G. R. Hawley, and M. B. Welch, Macromolecules **33**, 6861 (2000).
[38] A. Winkel, Internet Website: SPM Image Gallery (Scanning Probe Microscopy at Bristol; http://spm.phy.bris.ac.uk/).
[39] J. D. Hoffman and J. J. Weeks, J. Res. Natl. Bur. Stand., Sect. A **66**, 13 (1962).
[40] J. W. Cahn and J. E. Hillard, J. Chem. Phys. **28**, 258 (1958).
[41] S. M. Allen and J. W. Cahn, Acta Metall. **27**, 1085 (1979).
[42] P. R. Harrowell and D. W. Oxtoby, J. Chem. Phys. **86**, 2932 (1987).
[43] *Polymer Handbook*, edited by J. Brandrup, E. H. Immergut, E. A. Grulke, A. Abe, and D. R. Bloch (Wiley, New York, 1999).
[44] J. I. Lauritzen, Jr., and J. D. Hoffman, J. Appl. Phys. **44**, 4340 (1973).
[45] J. Rodriguez-Arnold, A. Zhang, S. Z. D. Cheng, A. Lovinger, E. T. Hsieh, P. Chu, T. W. Johnson, K. G. Honnell, R. G. Geerts, S. J. Palakal, G. R. Hawley, and M. B. Welch, Polymer **35**, 1884 (1994).